

See discussions, stats, and author profiles for this publication at: <https://www.researchgate.net/publication/329309781>

# Experimental and numerical analysis on the bending response of the geometrically gradient soft robotics actuator

Article in Archives of Mechanics · January 2018

DOI: 10.24423/aom.2903

CITATIONS

2

READS

29

3 authors, including:



Assoc. Prof. Savas Dilibal  
Istanbul Gedik University

18 PUBLICATIONS 109 CITATIONS

[SEE PROFILE](#)



Haydar Sahin  
Gedik Üniversitesi

6 PUBLICATIONS 36 CITATIONS

[SEE PROFILE](#)

Some of the authors of this publication are also working on these related projects:



Nickel-titanium shape memory alloy-actuated thermal overload relay [View project](#)



Antagonistic Nickel-Titanium Shape Memory Alloy Actuators [View project](#)

## Experimental and numerical analysis on the bending response of the geometrically gradient soft robotics actuator

S. DILIBAL<sup>1)</sup>, H. SAHIN<sup>1)</sup>, Y. CELIK<sup>2)</sup>

<sup>1)</sup>*Mechatronics Engineering Department  
Istanbul Gedik University  
Kartal Istanbul, Turkey  
e-mails: savas.dilibal@gedik.edu.tr, haydar.sahin@gedik.edu.tr*

<sup>2)</sup>*BIAS Engineering Inc.  
Istanbul, Turkey*

IN THIS STUDY, THREE DIFFERENT SOFT PNEUMATIC ACTUATORS (SPA) are designed and directly fabricated through additive manufacturing using thermoplastic polyurethane (TPU) filaments. The equal total inner volume size is used in the three varied designs to compare their effect on the bending response. A material model is selected and implemented according to the uniaxial tensile test parameters. The experimental results obtained from three different soft pneumatic actuators are compared with numerical model results. Especially, the experimentally measured bending forces are compared with the numerical model counterparts. The highest continuous bending deformation is determined among the three different soft pneumatic actuators. Additionally, a new integrated design and manufacturing approach is presented aiming to maximize the potential bending capability of the actuator through additive manufacturing.

**Key words:** thermoplastic elastomers, bending response, soft robotics actuator, additive manufacturing, hyperelastic material models.

Copyright © 2018 by IPPT PAN

### 1. Introduction

THE ELASTOMERIC MATERIALS BASED SOFT INFLATABLE ACTUATORS change dramatically the mechanism and structure of the robotics systems [1]. The hyperelastic characteristics of the materials provides the large deformation under loading. Upon unloading, the elastomeric materials revert back to the initial shape with a minimum permanent deformation. Their flexible structures provide a high degree of freedom with a lightweight mechanism compared to the rigid components. These types of soft robotics systems are started to be used in many fields, such as biomedical and industrial areas. They are mainly used for the rehabilitation purposes in the biomedical field [2]. Alternatively, they

are assembled with the industrial manipulators for grasping delicate or complex objects in industry [3–5].

Many soft robotics systems are manufactured using a conventional casting process. The mold which is printed using fused deposition modelling (FDM) is commonly used in manufacturing of the soft robotics components [4–8]. However, the difficulties of the complex mold design, the inconsistent feature of the casting process, the multiple production steps are the main drawbacks of the casting based soft robotics systems. Thus, the additive manufacturing technique replaced the casting technique to fabricate directly the soft components. The additive manufacturing process enables to have a complex soft robotics actuator design with a high precision [9–11]. In addition, the additive manufacturing process can integrate design and manufacturing approach to build new actuators, such as artificial muscles [12, 13], biologically inspired robots [14] and lightweight soft robots [15].

Most of the soft pneumatics actuators (SPA) are actuated using the pressurized fluid flow by inflating the flexible chambers. The main advantage of the soft inflatable actuator system is the establishment of the equally distributed forces on the surface of the varied geometrical chamber shapes. Additionally, the soft pneumatics actuators have cost effective maintenance and replacements compared to the other fluidic systems [10]. Their bending motion performance are dependent on the material property, the asymmetric structural design and the applied pressure value [11]. The asymmetry in design plays an important role to achieve the desired bending motion [16, 17]. It can be classified into two types which are geometry and material based asymmetry. The details of the actuation type for bending of the soft pneumatic actuators are depicted in Fig. 1.

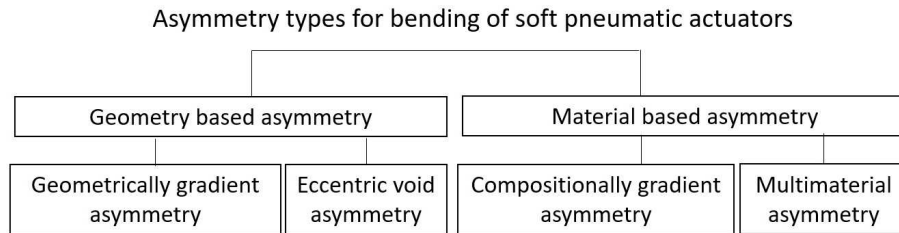


FIG. 1. Types of asymmetry for bending response of soft pneumatic actuators.

Soft robots have two major characteristics which are continuum body motion and large-scale deformation. The asymmetric shell pattern design with fixed-end boundary conditions provides the required bending motion with large-scale deformation. Compared to the other asymmetry types, the geometrically gradient asymmetry is mainly used for achieving the maximum bending motion [9, 10]. Most of the soft robotics actuators are made of materials with hyperelastic

characteristics which allow large-scale deformation. The stress-strain relationship of these materials can be defined by means of strain energy function. The strain energy function can be stated in terms of strain invariants which is also a function of principal stretch ratios [18]. Herrmann and coworkers [19, 20] made the calculation of displacement through the variational theorem for the nearly-incompressible elastomeric material.

The effect of the geometrical design on the bending motion should be systematically analyzed to specify the performance of the soft pneumatics systems. In this study, the effect of geometrically gradient asymmetry is investigated using equal total inner volume sized three different soft robotics actuators. The experimental results and model predictions are analyzed to compare maximum bending deformation for each manufactured actuator.

## 2. Materials, manufacturing process and design

Thermoplastic polyurethane (TPU) filaments with the diameter of 1.75 mm are used for the additive manufacturing of the soft robotics actuator. A systematic flowchart which is depicted in Fig. 2 is followed for the actuator manufac-

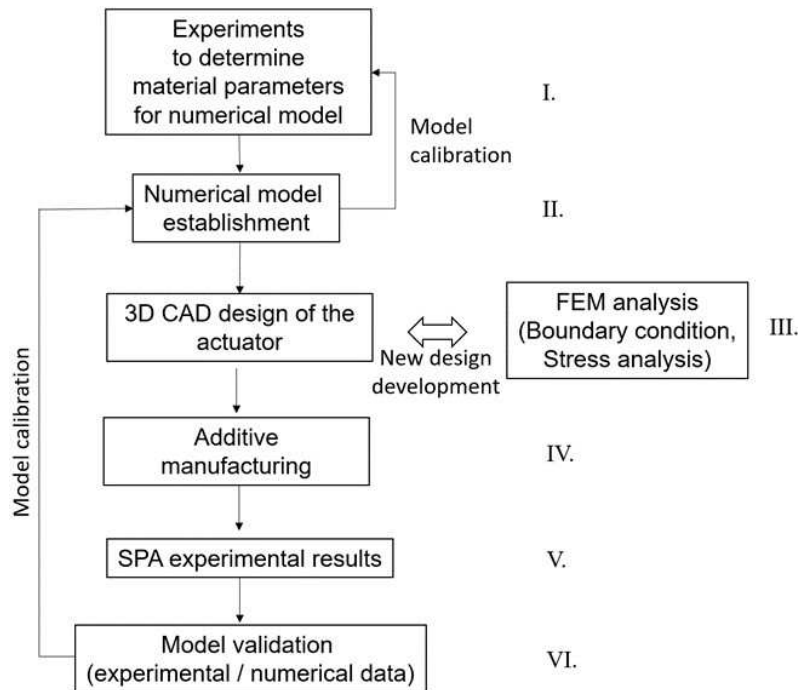


FIG. 2. Schematic of manufacturing process for the developed soft pneumatic actuator prototype.

turing process. The determination of the material parameters for a numerical model is obtained through the tensile tests which is explained in the following subsection.

### 2.1. Experiments to determine material parameters for numerical model

The uniaxial tensile tests are conducted using TPU dog-bone samples. The tensile test results are used to generate the material parameters of the numerical model. The dog-bone samples of the uniaxial tensile tests are prepared according to the ISO 37-2011 standard. The loading rate of 200 mm/min is applied to conduct the tensile tests. Young's Modulus and Shore A hardness values were obtained as 8 MPa and 94A from the experimental results. The numerical model is designed using the experimental result of the tensile test of the TPU dog-bone samples.

### 2.2. Numerical model establishment

In order to create material models for numerical analysis, the strain and stress values which were obtained from the uniaxial tensile test were used as an input in Marc Mentat (MSC Software Corporation) experimental data fit tool. Three different hyperelastic material models which are neo-Hookean model, Mooney–Rivlin model and Ogden model were used for predicting the nonlinear stress-strain behavior of a material. The parameter values for hyperelastic material models are shown in Table 1. The strain energy function of a hyperelastic material model for the neo-Hookean model is shown in Eq. (2.1). The strain energy function of a hyperelastic material model for the Mooney–Rivlin model is shown in Eq. (2.2). The strain energy function of a hyperelastic material model for the Ogden model is shown in Eq. (2.3). In the equations, the parameters of  $I_1$ ,  $I_2$  are the strain invariants. The parameters of  $\lambda_1^{\alpha_k}$ ,  $\lambda_2^{\alpha_k}$ ,  $\lambda_3^{\alpha_k}$  and are the principal stretch ratios for the Ogden model.

$$(2.1) \quad W_{\text{neo-Hookean model}} = C_{10} \cdot (I_1 - 3),$$

$$(2.2) \quad W_{\text{Mooney-Rivlin model}} = C_{10} \cdot (I_1 - 3) + C_{01} \cdot (I_2 - 3),$$

$$(2.3) \quad W_{\text{Ogden model}} = \sum_{k=1}^N \frac{\mu_k}{\alpha_k} \cdot (\lambda_1^{\alpha_k} + \lambda_2^{\alpha_k} + \lambda_3^{\alpha_k} - 3).$$

The material specific constants that can be seen in Table 1 were derived using experimental data fit tool. The Finite Element Model (FEM) of a dog-bone specimen was created to select the convenient material model. The FEM for this analysis consists of 74750 eight-noded hexahedral elements (HEX8). All elements are of type 84 with full integration formulation. Type 84 elements are eight-node isoparametric elements with an additional node for the pressure. The

pressure is assumed constant throughout the element. This type of elements support incompressibility, which is needed in the hyperelastic material behavior. The front view of a FEM of dog-bone specimen is shown in Fig. 3.

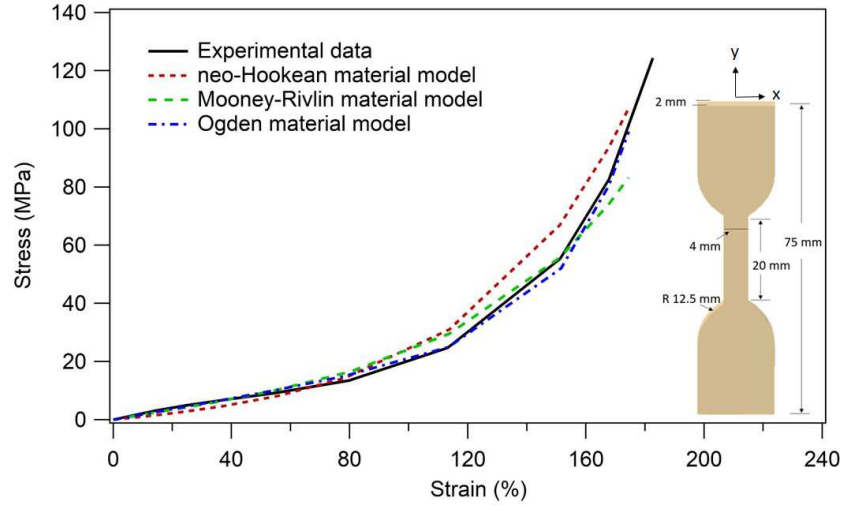


FIG. 3. True stress versus true strain plots for the uniaxial tensile test, the hyperelastic material models and related tensile test specimen.

FEM analyses were run for each material model. The true strain versus true stress plots for the node which is located in the middle of a dog-bone specimen are used for the comparison. The model results shown in Fig. 3 revealed that the Ogden hyperelastic constitutive material model converges with the uniaxial

**Table 1. Parameter values for hyperelastic material models.**

Parameters	Hyperelastic material model types		
	Ogden model	neo-Hookean model	Mooney–Rivlin model
$C_{01}$ , $C_{10}$ : Material specific constants derived from experimental data	—	1.64745	0.930759, 1.99405
K: Bulk modulus	30063.9	16474.5	29248.1
LSE: Least square error	0.0729091	0.698497	0.214687
N: Number of terms selected to create the material model	2	—	—
$\mu_k$ : Material specific moduli derived from experimental data	0.0334692, 4362.65	—	—
$\alpha_k$ : Material specific exponents derived from experimental data	4.36501, 0.00272299	—	—

tensile test results more convenient than the other hyperelastic models. Hence, this constitutive model is selected as a convenient material model for the FEM analysis of the soft actuator structures.

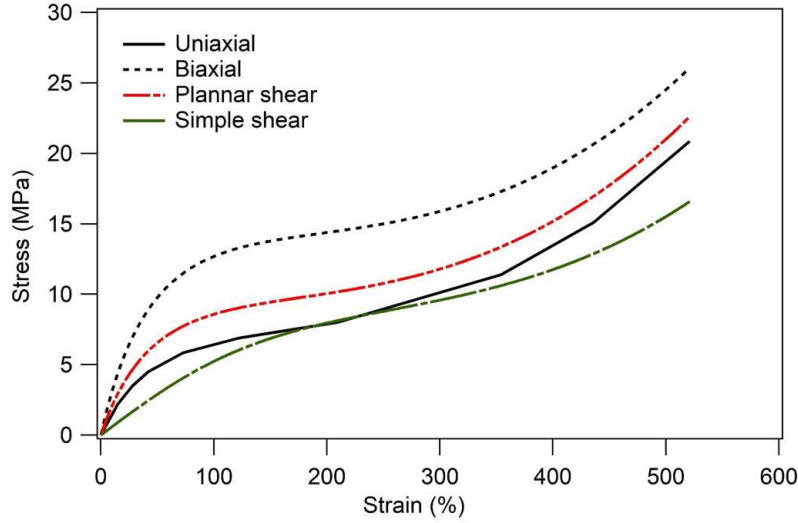


FIG. 4. Engineering stress versus engineering strain responses for the Ogden material model.

Uniaxial, biaxial, planar shear and simple shear behaviors of the Ogden constitutive material model are shown in Fig. 4. A number of terms taken into consideration ( $N$ ) is 2. Moduli are  $\mu_1 = 0.0334692$  MPa and  $\mu_2 = 4362.65$  MPa and exponents are  $\alpha_1 = 4.36501$  and  $\alpha_2 = 0.00272299$ .

### 2.3. The 3D CAD design of the actuator

The three varied designs with an equal total inner volume value of the chamber size is used for the experimental setup to have pneumatically equivalent systems for comparison purposes. The soft robotics actuator with three different trapezoidal geometries are designed as shown in Fig. 5. The soft actuators with the taper angle of  $8.3^\circ$ ,  $0^\circ$  and  $-8.3^\circ$  are used in the designs. The total chamber size volume for each of the designs is measured as  $8.89 \text{ cm}^3$ . The actuators having  $0^\circ$ ,  $8.3^\circ$  and  $-8.3^\circ$  are called SPA-1, SPA-2 and SPA-3, respectively. The developed designs are used to fabricate soft pneumatic actuator prototypes through the FDM process. The same fused deposition manufacturing parameters are selected during fabrication. An equal pneumatic pressure value in the range of  $0.1 \text{ MPa}$ – $0.5 \text{ MPa}$  are applied for the bending performance comparison.

The bending motion for the soft actuator structure is emerged from the geometrically asymmetric design concept. The bending of a soft pneumatic actuator occurs through expanding of the top and stretching the walls of the chamber as

shown in Fig. 6. The actuator chambers are filled with pressurized air. The inflation of the flexible inner chambers causes the bending motion of the soft actuator. Each soft actuator consists of the extensible and inextensible layers.

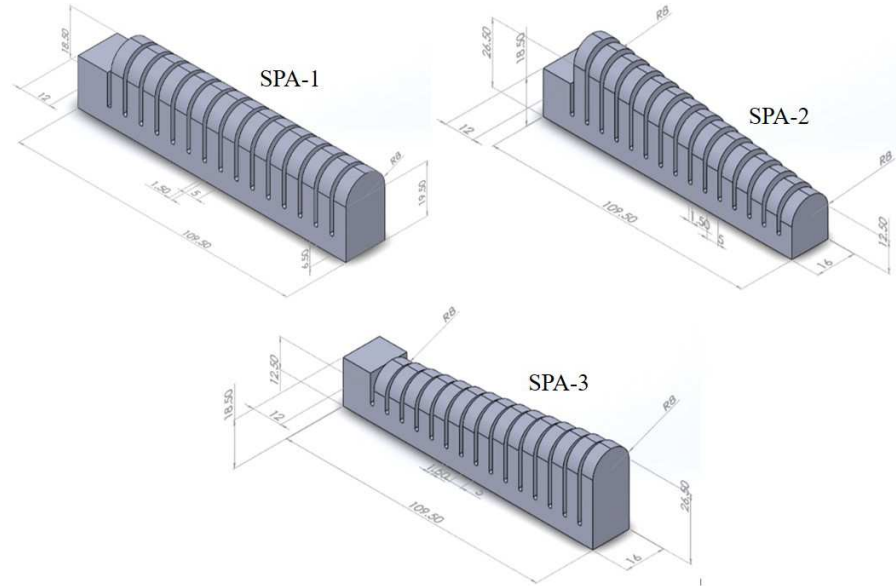


FIG. 5. Soft robotics actuator designs with three different trapezoidal geometries.

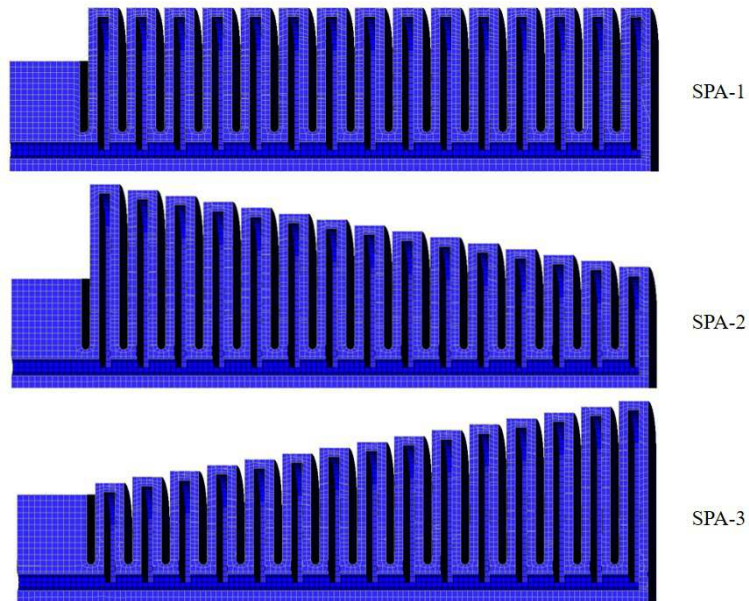


FIG. 6. The cross-sectional area view of the SPA-1, SPA-2 and SPA-3.



The extensible layer provides the bending of the soft actuator. The change in the chamber volume size defines the time interval for reaching the maximum bending angle. The extensible layers cause the bending motion by applying force against each other.

#### 2.4. FEM analysis

Numerical models of the SPA structures were built using Marc Mentat (MSC Software Corporation). Details of finite element models are given in Table 2. In order to mesh the structure of the actuators, eight-node hexahedral elements (HEX8) are used. After conducting the mesh convergence, an average element length of 1 mm is determined. Additionally, type 84 with full integration of the Herrmann element is selected as the element type.

**Table 2. Details of FEM.**

	Number of elements	Number of nodes
SPA-1	54649	74810
SPA-2	57917	78846
SPA-3	57783	78572

The nodes located on the outer surface of base of the actuators are constrained in all directions to satisfy the fixed-end boundary conditions. The surfaces of the elements that are exposed to pressure are defined as a cavity. A cavity pressure having the maximum value of 0.5 MPa is defined as a ramp input to simulate pneumatic pressure from 0.1 to 0.5 MPa. The large strain and large deformation formulation is used for a nonlinear procedure. The follower force option for a pressure load in Marc is activated to simulate cavity pressure accurately. The cavities of SPA-1, SPA-2 and SPA-3 are shown through the cross-sectional area view in Fig. 6. Each actuator is defined as a deformable contact body. The friction coefficient for the self-contact condition is defined as 0.5.

#### 2.5. Experimental setup with corresponding numerical design

To compare the experimental system with the equivalent numerical model, the numerical model is established as similar to the experimental setup. In order to compare the free-expansion behavior of the actuator structures, the FEM of each SPA are prepared and run as in the experimental system. In these analyses, the bending deformation of SPAs with respect to the cavity pressure is received as an output in order to compare with the free expansion experimental results. Afterwards, a geometrical surface, defined as a rigid body, is located 25 mm away from the tip of the SPAs in z direction to measure the bending forces. For each SPA, this analysis configuration is set and the contact body force between

a rigid surface and SPA with respect to the cavity pressure is taken as an output in Marc Mentat (MSC Software Corporation).

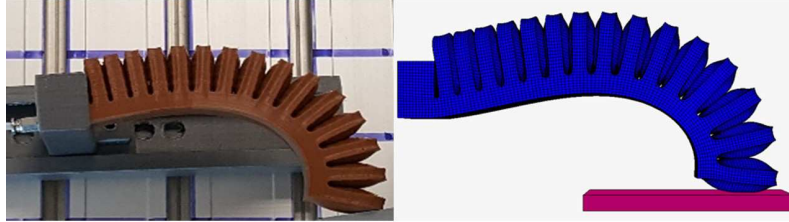


FIG. 7. Experimental setup and corresponding numerical design with boundary condition for the applied force measurements of the SPA-1.

A load-cell is used to measure the experimental bending force received from the soft inflatable actuator as shown in Fig. 7. The pneumatic fluid pressure is applied into the numerical model to analyze the bending response of three different actuators for comparison purposes.

### 3. Experimental and numerical results

The experimental results which are obtained from the experimental setup are investigated based on the bending displacement and the bending force for the three SPA designs. The numerical results which are generated by finite-element modelling are compared with the experimental results.

To observe the comparison of the bending displacements, the experimental and numerical results are placed in Fig. 8. Each bending curve and bending displacement are obtained from the applied pressures of 0.1, 0.3 and 0.5 MPa. The increase of the value of the applied pressure causes the gradual increase in the bending motion and displacement.

Considering the combined results presented in Fig. 8, a number of remarks can be obtained as follows. Both experimental measurements and model predictions indicate that the SPA-2 shows the highest bending deformation compared to the SPA-1 and SPA-3 designs. In particular, the bending deformation increases gradually by the value of pressure which are 0.1, 0.3 and 0.5 MPa.

The contact force of the actuator is measured using a load-cell as a rigid surface. Experimental results and model predictions for bending forces are shown in Fig. 9. The maximum contact force between the actuator and the surface, which is called as the bending force, is the highest for SPA-2 compared to the SPA-1 and SPA-3. Particularly, the force exerted by SPA-2 is 30% and 89% higher than SPA-1 and SPA-3, respectively.



















Experimental/ Model Results		Applied Pressure		
		0.1 MPa	0.3 MPa	0.5 MPa
SPA-1	Experimental result			
	Model result			
SPA-2	Experimental result			
	Model result			
SPA-3	Experimental result			
	Model result			

FIG. 8. Comparison of the bending deformation of experimental results and model predictions.

The bending deformation obtained from the experimental results and the model predictions for the chamber pressure of 0.1 MPa–0.5 MPa are shown

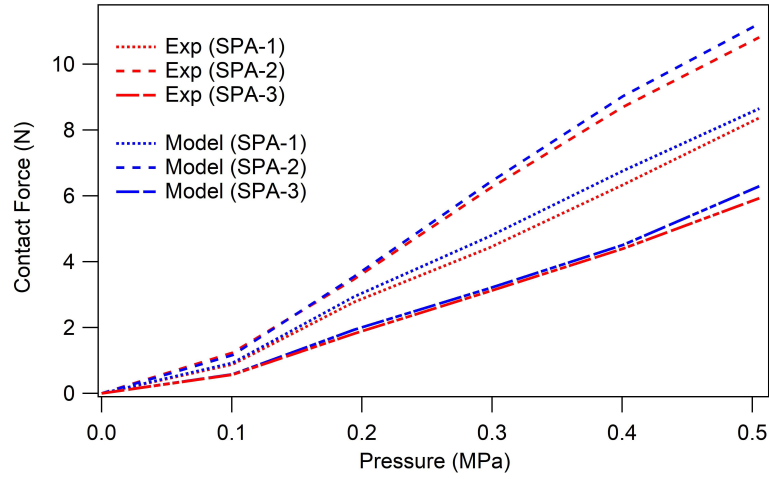


FIG. 9. Pressure vs applied force plots extracted from experimental and corresponding numerical results for each soft actuator design.

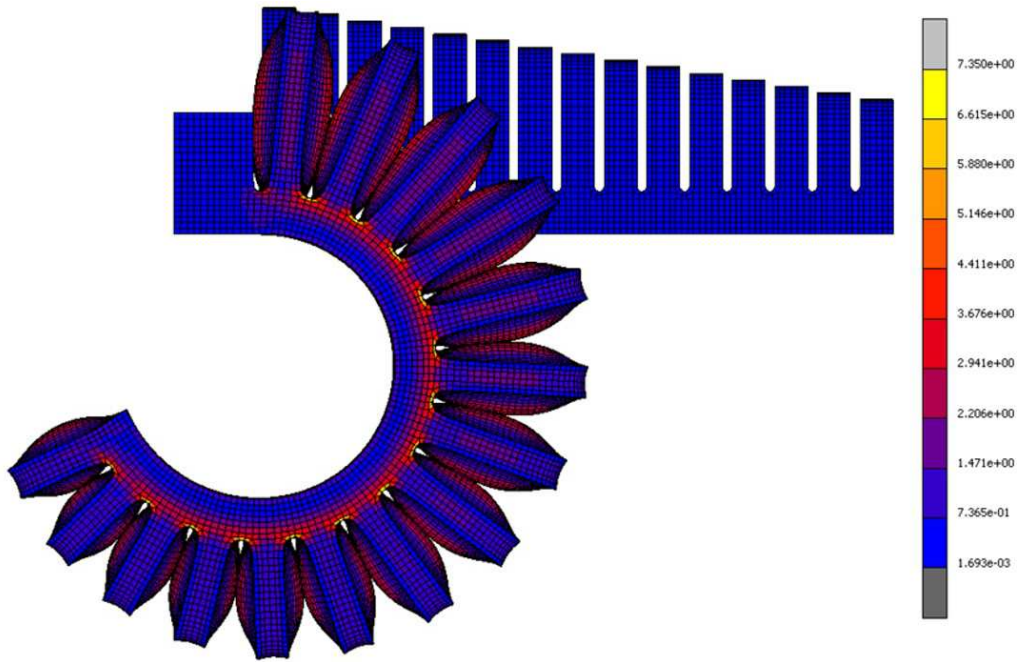


FIG. 10. Cauchy (true) stress values of SPA-2 from 0 to 0.5 MPa.

in Fig. 8. The maximum bending force occurs in SPA-2 design as it is seen in Fig. 9. The finite element analysis of SPA-2 with details of Cauchy stress values is described from 0 to 0.5 MPa in Fig. 10.

#### 4. Discussion

The geometrically gradient chamber design for the bending of a soft robotic actuator is thoroughly investigated here. The desired bending can be achieved by the structural asymmetry in the design. This geometry based asymmetric structure is conceived by the systematic design process of the actuator to obtain dedicated bending actuation. Other than the geometry based asymmetry, the material based asymmetry is also used for the soft robotic actuator in the literature [21].

Considering the bending response of the soft pneumatic actuator structures, the SPA-2 showed the highest bending response compared to the other designs. This result is compatible with the bio-mimicking concept if the elephant nose is observed. It is clear that the elephant's trunk-inspired the design of a cylindrical diameter which gradually reduces through the trunk-tip, similar to the SPA-2 design [22]. The free-end geometry of the SPA-2 design is the smallest among the SPA designs. It is preferred due to the potential easy-access capability in narrow and tight workspaces.

The majority of the soft robotic actuator applications are designed using the casting technique. The casting technique uses the silicone as a material which is convenient for the mass production. The high bending response can be obtained from the casting based soft actuators. The Ecoflex 30 material with Shore hardness of 30A is commonly used for soft actuator [3]. UDUPA *et al.* [7] studied the soft actuator made of silicone materials which applies the maximum force of 0.17 N under the pressure value of 180 kPa. However, the applied bending force is higher in TPU based additively manufactured soft actuator compared to the casting processed soft actuator. In the experimental results of this study, the maximum applied bending force is measured as 12 N for the TPU based additively manufactured soft actuator.

In model prediction, different material models were developed to obtain maximum consistency with experimental results. For instance, the Ogden material model result matches with the experimental result conducted by KUT *et al.* [23]. They revealed that the Ogden material model gives the closest result to the experimental counterpart for the bending motion. In this respect, the Ogden material model predicted coherently the bending motion of the manufactured soft robotics actuator structure compared to the other material model predictions in this study.

#### 5. Conclusions

In this paper, the effect of geometrical asymmetry on the bending response of the three different soft pneumatic actuators is examined using experimental

and numerical analyses. Each of the soft inflatable actuator has been designed and fabricated with an equal total inner volume size. Among the hyperelastic material models, the Ogden model uses the principal stretches to predict large deformations. The Ogden constitutive model was determined as a convenient constitutive material model for the mechanics of hyperelastic material based structures. The following conclusions were made for the experimental results and numerical counterparts.

A significant difference in bending responses was observed for the designs of SPA-1, SPA-2 and SPA-3. The SPA-2 is the most convenient design for satisfying the high force requirement of 12 N.

Both the experimental results and numerical model prediction of the pneumatic soft actuator demonstrated similar bending responses under the equally applied inner pressure values of 0.1–0.5 MPa.

A greatest bending response was obtained on the tip of the SPA-2 design in both experimental and modeling results.

Additionally, SPA-2 is the most convenient soft robotic actuator design to manipulate in a small working space, such as minimally invasive surgeries.

## References

1. Z. WANG, M. ZHU, S. KAWAMURA, S. HIRAI, *Comparison of different soft grippers for lunch box packaging*, Robotics and Biomimetics, **4**, 1–9, 2017.
2. H. ZHANG, Y. WANG, M.Y. WANG, J.Y.H. FUH, A.S. KUMAR, *Design and analysis of soft grippers for hand rehabilitation*, Proceeding of ASME 12th International Manufacturing Science and Engineering Conference, June 4–8, LA, CA, U.S.A., 2017.
3. M. BOBAK, P. POLYGERINOS, C. KEPLINGER, S. WENNSTEDT, R.F. SHEPHERD, U. GUPTA, J. SHIM, K. BERTOLDI, C.J. WALSH, G.M. WHITESIDE, *Pneumatic networks for soft robotics that actuate rapidly*, Advanced Functional Materials, **24**, 2163–2170, 2014.
4. B. GORISSEN, D. REYNAERTS, S. KONISHI, K. YOSHIDA, J. KIM, M.D. VOLDER, *Elastic inflatable actuators for soft robotic applications*, Advanced Materials, **29**, 1–14, 2017.
5. A. FRICK, M. BORM, N. KAoud, J. KOLODZIEJ, J. NEUDECK, *Microstructure and thermomechanical properties relationship of segmented thermoplastic polyurethane*, AIP Conference Proceedings, **1593**, 520–525, 2014.
6. M.A. ABD, C. ADES, M. SHUQIR, M. HOLDAR, M. AL-SAIDI, *Impacts of soft robotic actuator geometry on end effector force and displacement*, 30th Florida Conference on Recent Advances in Robotics, May 11–12, Florida Atlantic University, Boca Raton, 2017.
7. G. UDUPA, P. SREEDHARAN, P.S. DINESH, D. KIM, *Asymmetric bellow flexible pneumatic actuator for miniature robotic soft gripper*, Journal of Robotics, **1**, 1–11, 2014.
8. J. HUGHES, U. CULHA, F. GIARDINA, F. GUENTHER, A. ROSENDO, F. LIDA, *Soft manipulators and grippers: a review*, Frontiers in Robotics and AI, **3**, 69, 1–12, 2016.
9. M. TROLLEY, R.F. SHEPHERD, M. KARPELSON, N.W. BARTLETT, K.C. GALLOWAY, M. WEHNER, G.M. WHITESIDES, R.J. WOOD, *An untethered jumping soft robot*, IEEE/RSJ International Conference on Intelligent Robots and Systems (IROS), September 14–16, Chicago, 2014.

10. Y. SUN, Y.S. SONG, J. PAIK, *Characterization of silicon rubber based soft pneumatic actuators*, IEEE/RSJ International Conference on Intelligent Robots and Systems (IROS), November 3–7, Tokyo, 2013.
11. J.H. LOW, W.W. LEE, P.M. KHIN, N.V. THANKOR, S.L. KUKREJA, H.L. REN, C.H.E YEOW, *Hybrid tele-manipulation system using a sensorized 3D-printed soft robotic gripper and a soft fabric-based haptic glove*, IEEE Robotics and Automation Letters, **2**, 2, 2017.
12. H. RODRIGUE, W. WANG, D. KIM, S. AHN, *Curved shape memory alloy-based soft actuators and application to soft gripper*, Composite Structures, **176**, 398–406, 2017.
13. B.N. PEELE, T.J. WALLIN, H. ZHAO, R.F. SHEPHERD, *3D printing antagonistic systems of artificial muscle using projection stereolithography*, Bioinspiration & Biomimetics, **10**, 1–8, 2015.
14. D. TRIVEDI, C.D. RAHN, W.M. KIER, I.D. WALKER, *Soft robotics: biological inspiration, state of the art, and future research*, Applied Bionics and Biomechanics, **5**, 99–117, 2008.
15. A. ALBU-SCHAFER, O. EIBERGER, M. FUCHS, M. GREBENSTEIN, *Soft robotics: from torque feedback controlled lightweight robots to intrinsically compliant systems*, IEEE Robotics & Automation Magazine, **15**, 20–30, 2008.
16. R. MUTLU, S.K. YILDIZ, G. ALICI, M. PANHUIS, G.M. SPINKS, *Mechanical stiffness augmentation of a 3D printed soft prosthetic finger*, IEEE International Conference on Advanced Intelligent Mechatronics, Banff, Alberta, Canada, July 12–15, 2016.
17. A. PRZYBYTEK, J. KUCINSKA-LIPKA, H. JANIK, *Thermoplastic elastomer filaments and their application in 3D printing*, Elastomery, **4**, 32–39, 2016.
18. M. SHAHZAD, A. KAMRAN, M.Z. SIDDIQUI, M. FARHAN, *Mechanical characterization and FE modelling of a hyperelastic material*, Materials Research, **5**, 918–924, 2015.
19. R.L. TAYLOR, K.S. PISTER, AND L.R. HERRMANN, *On a variational theorem for incompressible and nearly-incompressible orthotropic elasticity*, International Journal of Solids Structures, **4**, 875–883, 1968.
20. L.R. HERRMANN, *Elasticity equations for incompressible and nearly incompressible materials by a variational theorem*, AIAA Journal, **3**, 1896–1900, 1965.
21. B.S. SHARIAT, Q. MENG, A.S. MAHMUD, Z. WU, R. BAKHTIARI, J. ZHANG, F. MOTAZEDIAN, H. YANG, G. RIO, T. NAM, Y. LIU, *Functionally graded shape memory alloys: Design, fabrication and experimental evaluation*, Materials and Design, **124**, 225–237, 2017.
22. R. BEHRENS, M. POGGENDORF, E. SCHULENBURG, N. ELKMANN, *An Elephant's Trunk-Inspired Robotic Arm – Trajectory Determination and Control*, 7th German Conference on Robotics, Proceedings of Robotik, Munich, 2012.
23. S. KUT, G. RYZINSKA, B. NIEDZIALEK, *Numerical analysis and experimental verification of elastomer bending process with different material models*, Open Engineering, **6**, 228–234, 2016.

Received February 12, 2018; revised version July 2, 2018.